ISSN 2070-2051, Protection of Metals and Physical Chemistry of Surfaces, 2016, Vol. 52, No. 1, pp. 104–110. © Pleiades Publishing, Ltd., 2016.

NANOSCALE AND NANOSTRUCTURED MATERIALS AND COATINGS

Corrosion Behaviour of Polycrystalline Nb_2O_5 thin Films and its Size Effects[1]

F. B. Destro[a,*], M. Cilense[b], M. P. Nascimento[a], F. González Garcia[c], L. R. O. Hein[a], and A. Z. Simões[b]

[a] *Universidade Estadual Paulista- Unesp—Faculdade de Engenharia de Guaratinguetá, Av. Dr. Ariberto Pereira da Cunha, 333, Bairro Pedregulho, CEP 12516-410, Guaratinguetá-SP, Brazil*

[b] *Laboratório Interdisciplinar em Cerâmica (LIEC), Departamento de Físico-Química, Instituto de Química, UNESP, CEP: 14800-900, Araraquara, SP, Brazil*

[c] *Universidade Federal de Itajubá, Instituto de Física e Química, Av. BPS 1303, Bairro Pinherinho, CEP 37500-903, Itajubá, MG, Brazil*

e-mail: fabricio_feg_unesp@yahoo.com.br

Received Match 10, 2015

Abstract—This study examines the effect of film thickness ranging from 230 to 404 nm on the corrosion resistance of Nb_2O_5 thin films grown by chemical solution deposition. The films were characterized to obtain the relationships between the deposition parameters and the most relevant physical properties (structural, surface morphology and corrosion resistance). From X-ray diffraction and XPS analyses we can conclude that the films were stoichiometric Nb_2O_5 and crystalline. The internal strain and morphology of the film changes as the number of layers increases indicating a thickness dependent grain size. The surface roughness, corrosion resistance were also affected by the film thickness. Electrochemical impedance spectroscopy (EIS) shows that the thicker film have higher passive and charge transfer resistance than the control samples. These results coating layer of Nb_2O_5 improves the corrosion resistance on an API 5L X80 steel alloy due to the formation of a film on the surface.

DOI: 10.1134/S2070205116010081

1. INTRODUCTION

Low alloy steel has low cost and high strength. However, the poor corrosion resistance is still questionable to most chemicals and environmental application. It has been continually investigated to improve the corrosion problem in order to maintain their advantages [1–14]. In addition, low alloy steels are widely used to manufacture large engineering structures, such as flue gas desulfurization (FGD) [15]. The steel chemistry and processing techniques need to be designed carefully to achieve a good corrosion resistance. It is believed that Nb_2O_5 can increase the strength of steel without any significant loss of both ductility and toughness and improves the resistance to localized corrosion [16–20]. Furthermore, it has a good combination of thermal fatigue resistance, high temperature strength, and corrosion resistance in automotive exhaust systems [21–24]. Niobium pentoxide can be reduced to a lower oxide and to metallic niobium. However, the electrochemical reduction of Nb_2O_5 in aqueous solutions in the absence of a complexing agent is difficult [25]. In addition, when alloys of niobium and various metals, such as Ti, Cr, Al, and Mo, are exposed to oxidizing conditions, the mixed oxides formed at surface affect the electrode potential and corrosion resistance of the alloys [26]. As Nb oxides have a significant effect on the corrosion resistance and mechanical properties of low alloy steel, it is important to examine the effect of Nb_2O_5 coating to these low alloy steels. Therefore, Nb_2O_5 is considered to be a good coating protection element to improve the corrosion behavior of steel, already being a material researched for improving corrosion resistance in biomedical applications [27]. The size effects of thin films are different from that of bulk materials. Size effects of thin films include not only grain size but also film thickness. It is difficult to distinguish the size effects derived from grain size from those derived from film thickness because the grain size of thin films generally changes with film thickness if films are prepared from chemical solution deposition [28]. Furthermore, it has also been reported that the film thickness dependence of a polycrystalline film is different from that of epitaxially grown films [29]. This study examined the corrosion performance of Nb_2O_5 containing low alloy steels as a function of thickness. The corrosion resistance of the steels was characterized by electrochemical impedance spectroscopy (EIS) measurements, X-ray photoelectron spectroscopy (XPS) and scanning electron microscopy (SEM). The roughness of the samples was obtained by confocal white light microscopy.

[1] The article is published in the original.

2. EXPERIMENTAL PROCEDURE

Niobium oxide (Aldrich, 98%) was used as raw material. The precursor solutions of niobium were prepared by adding the raw material to ethylene glycol and concentrated aqueous citric acid under heating and stirring. Appropriate quantities of solutions of Nb were mixed and homogenized by stirring at 90°C. The molar ratio of metal: citric acid: ethylene glycol was 1 : 4 : 16. The viscosity of the resulting solution was adjusted to 20 cP by controlling the water content using a Brookfield viscosimeter. Films were spin-coated from niobium citrate solution onto API 5L X80 steel substrates, which surfaces were prepared using emery paper 220 to 600 grade silicon carbide disk, and polished using a solution of 0.3 μm Al_2O_3 polishing (suspension in solution) as abrasive. Then the substrates were ultrasonically cleaned using acetone and ethanol for 15 minutes each. To achieve surface activation, a pretreatment at 500°C for 1 h was established before the deposition itself. Multilayered films were obtained by spinning 1, 2 and 4 times the deposition solution on the surface of the substrates. Each layer was annealed at 300°C for 1 hour with heating rate of 3°C/min in a conventional furnace and immediately crystallized at 650°C for 2 hours with heating rate of 5°C/min. All films were heat treated in static air. Phase analysis of the films was performed at room temperature by X-ray diffraction (XRD) using a Bragg-Brentano diffractometer (Rigaku-DMax 2500PC) and Cu-Kα radiation. The morphology of the annealed films was studied using scanning electron microscopy (Topcon SM-300). The Nb_2O_5 films surface was analyzed without any cover or special preparation and with incidence of secondary electrons detection while the thicknesses were measured from the transversal section. In this case back scattering electrons were utilized. The thickness results obtained from SEM represent an average value of three measurements. Surface average roughness (R_a) was examined by white light optical microscopy, using a Leica DCM3D microscope operating in confocal mode. For each condition (including the pure substrate), three random regions were analyzed. Next, a 0.5 mm diameter top Au electrode was sputtered through a shadow mask at room temperature. After deposition of the top electrode, the film was subjected to a post-annealing treatment in a tube furnace, at 300°C with constant heating rate of 1°C/min, in oxygen atmosphere for 1 hour. Here, the desired effect is to decrease eventually present oxygen vacancies. The XPS analysis was carried out at a pressure of less than 10^{-7} Pa using a commercial spectrometer (UNI-SPECS UHV) to verify the changes in surface chemical composition of the treated specimens. The Mg K line was used (h = 1253.6 eV) and the analyzer pass energy was set to 10 eV. The inelastic backgrounds of the Nb 3d electron core-level spectra were subtracted using Shirley's method. The composition of the near surface region was determined with an accuracy of ±10% from the ratio of the relative peak areas corrected by Scofield's sensitivity factors of the corresponding elements. The spectra were fitted without placing constraints using multiple Voigt profiles. The width at half maximum (FWHM) varied between 1.2 and 2.1 eV and the accuracy of the peak position was ±0.1 eV. EIS was carried out using a Parstat 2263 system with a commercial software program for the AC measurements. After the specimen reached a stable OCP, the EIS measurements were obtained with amplitude of 10 mV at frequencies ranging from 100 kHz to 10 mHz.

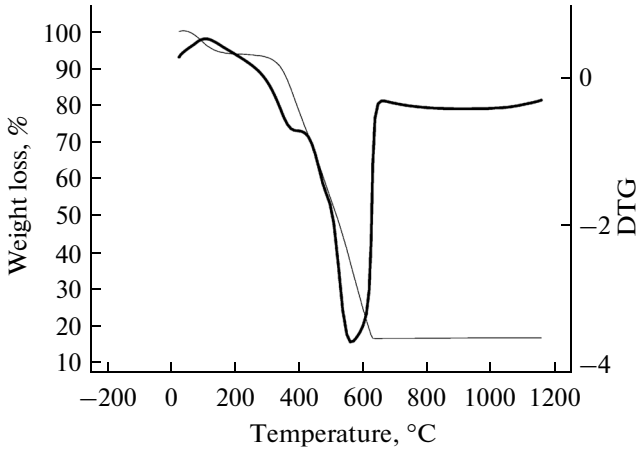

Fig. 1. TG/DTG curves of the Nb_2O_5 precursor powder obtained from room temperature up to 1200°C at a heating rate of 5°C/min.

3. RESULTS AND DISCUSSION

Figure 1 shows TG/DTG curves of the Nb_2O_5 precursor powder obtained from room temperature (20°C) up to 1200°C at a heating rate of 5°C/min. In this figure, three stages of weight loss can be observed. The first stage (from room temperature to 200°C) is related to the elimination of water produced during the esterification process and excess ethylene glycol. The second stage (200 to 400°C) corresponds to a break-away of polymeric chains formed by a polyesterification reaction and the last stage (between 400–600°C) is due to the decomposition of organic compounds. After this procedure, no weight loss can be detected because the decomposition of organic material is completed. A very intense exothermic signal observed in the range of 500–600°C was assigned to the pyrolysis of organic ligands and the main phase crystallization. Note that the Nb_2O_5 stable phase was formed above 600°C.

It is well known that properties of films are significantly affected by orientation of the underlying layer, film thickness and atmosphere flow. It is important to control the thickness of the layer due to its strong influence on the grain size, surface roughness and resistance corrosion. For thinner films interfacial layers which possess poor corrosion resistance could

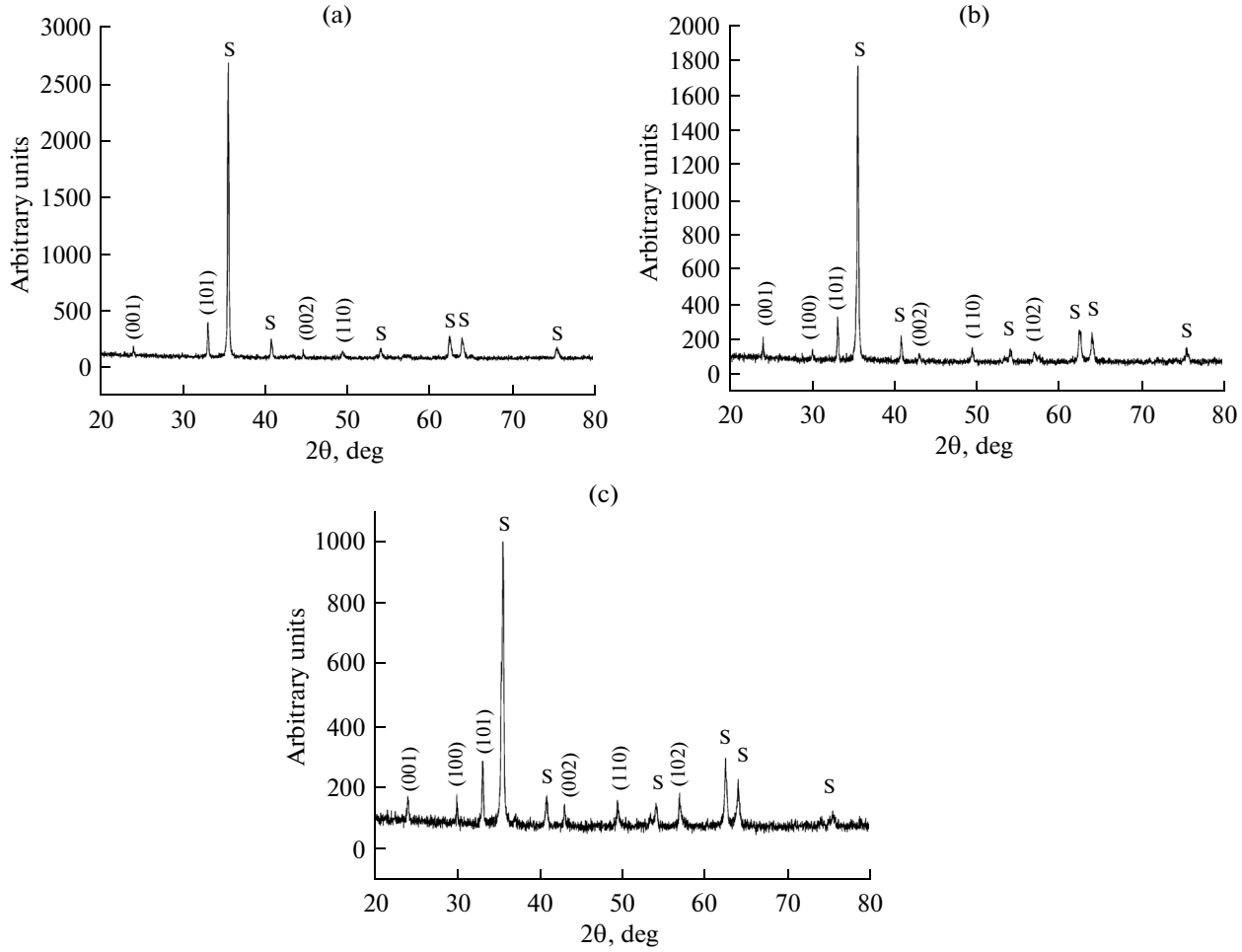

Fig. 2. XRD patterns for Nb_2O_5 phase films with different thicknesses: (a) 230, (b) 280 and (c) 404 nm.

appear at the interface film-substrate influencing on the performance of the device. These dead layers are originated from oxygen interdiffusion, chemical reaction, or structural defects and can be suppressed with thickness of films higher than 230 nm. Thus, films with 1, 2 and 4 layers were deposited and the XRD pattern is illustrated in Fig. 2a–2c, respectively. A single phase was observed regardless of the film thickness. The X-ray diffractogram apparently exhibits the niobium oxide to be crystalline in nature and possessing a hexagonal structure with the crystallite size in the range of 30–40 nm, in good agreement with previous data [30]. The characteristic peak for steel alloy substrate were also observed and denoted with the index "S". All films exhibit a polycrystalline structure and clearly showed diffraction peaks corresponding to the hexagonal Nb_2O_5 phase (JCPDS 28-0317) [31].

To estimate qualitatively the internal strain of Nb_2O_5 thin films, the full widths at half maximum (Δk) of XRD peaks were fitted for each peak with the scattering vector $\Delta k = (4\ \pi/\lambda)\ \sin\ \theta$ using a double Lorentzian function. An internal strain may be determined as follows equation (1):

$$\Delta k = 2\pi/D + (\Delta d/d)k, \quad (1)$$

where D is the effective grain size while $\Delta d/d$ is the internal strain derived from the Bragg relation.

The dependence of internal strain on film thickness is shown in Fig. 3. A minimum strain was obtained for the 280 nm (1 layer) thick film while the highest strain corresponds to both maximum and minimum thickness values. The origin of the strain in Nb_2O_5 thin films is addressed to the lattice distortion (b/a ratio) of the hexagonal phase. The suppressed lattice distortion might also cause internal strain in the film as observed in the thicker film. However, near a thickness of 300 nm the lattice distortion of Nb_2O_5 is reduced indicating that the driving force for the internal strain was minimized. The reason is that the internal strain changes the microstructure of Nb_2O_5 films. High internal strain corresponds to smaller and coarse grains and, as a result, provides an increase in the number of grain boundaries.

The thickness dependence of the a, b and c lattice constants and unit cell volume of the films is shown in Table 1. Nb_2O_5 films had a hexagonal structure over

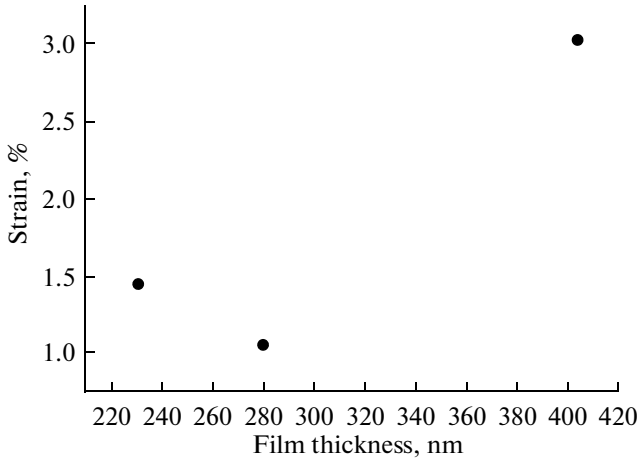

Fig. 3. Calculated internal strain for Nb_2O_5 phase thin films of various thicknesses.

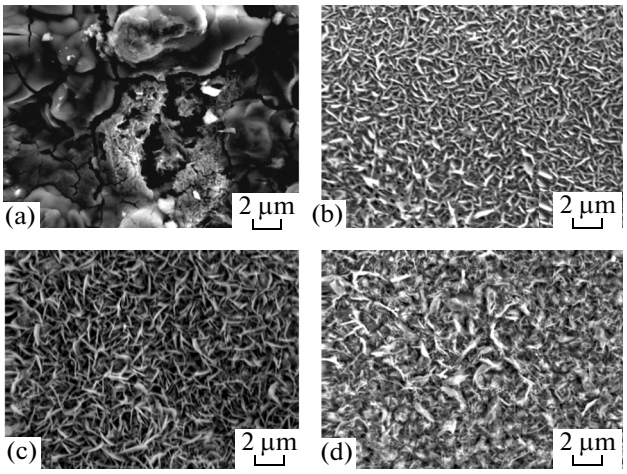

Fig. 4. SEM micrographs of niobium oxide coated on steel alloy substrates with different thicknesses: (a) pure substrate, (b) 230, (c) 280, and (d) 404 nm.

the entire thickness range investigated, although for thicker films there is a tendency to change from hexagonal to tetragonal structure once the a and b parameters becomes closer. In addition, there was a compressive stress in the in-plane dimension and the inner strain was gradually relaxed by the increase in the thickness because the *a*-axis slightly shortened and the *c*-axis elongated as the thickness increased. As a result, the volume of the unit cell hardly changed. The difference in crystalline properties and inner stress between Nb_2O_5 films on steel alloy substrates originates from the difference in the lattice mismatch, the thermal expansion coefficient and the crystalline structure.

Figure 4a shows a SEM micrograph of a typical region of the API 5L X80 steel substrate, while Figs. 4b–4d show SEM micrographs of niobium oxide coated on alloy steel substrate. The image shows that the film contains pores with varied diameter ranging from nanometer to micrometers with irregular granules. The mechanism for the formation of pores in a spin-coated polymeric precursor was assigned to the path of solvent evaporation during the calcinations process. The pores are interconnected with each other and there are not uniform in nature, the pore size varies from micrometer to nanometer level. The obtained porous microstructure depends upon the thermal treatment condition. During the thermal treatment, the organic residues were removed from the film and this result in the obtained porous morphology.

Figure 5a presents the roughness profile of a random region on the API 5L X80 steel while Figs. 5b–5d presents the images of the films with different thicknesses to evaluate average roughness using confocal mode. A strongly marked difference in the film microstructure can be observed for different numbers of layers, including the pure substrate without any deposition (just as a matter of differentiating the morphology). Figure 4a shows the pure substrate has a typical grain structure, assuming approximate spherical shape. When the film thickness increased, distinctive nanowhiskers were clearly observed. The absence of cracks and fissures indicates that the film presents a uniform microstructure. The thinner films present a dense microstructure. The difference in the shape of the grains is related to the amount of material deposited on the substrate surface to crystallize the films. Thinner films possess less material to be crystallized and the grains tend to assume the less elongated nanowhisker form. Meanwhile, when the film thickness increased, a large amount of material to be crystallized may lead to elongated nanowhisker grains (a less energetic). The root mean square roughness values were determined by analyzing several areas of the confocal images, excluding from the evaluation the deep trenches visible as black lines on the micrographs, that correspond to scratches of the substrate remaining after the polishing process. The standard deviation of the roughness values obtained from such determina-

Table 1. Dependence of a, b and c lattice constants and unit cell volume for Nb_2O_5 thin films as a function of thickness

	Parameter	230, nm	280, nm	404, nm
Refinement indexes	R_{wp} (%)	11.12	12.57	10.19
	R_{EXP}	7.06	9.00	7.02
	S	1.57	1.39	1.44
Lattice Parameters	a (Å)	5.4175	5.4141	5.4208
	b (Å)	5.4403	5.4377	5.4213
	c (Å)	32.7862	32.8409	32.8924
	V (Å^3)	966.30	966.85	966.4
	d (g/cm^3)	8.02	7.89	7.67

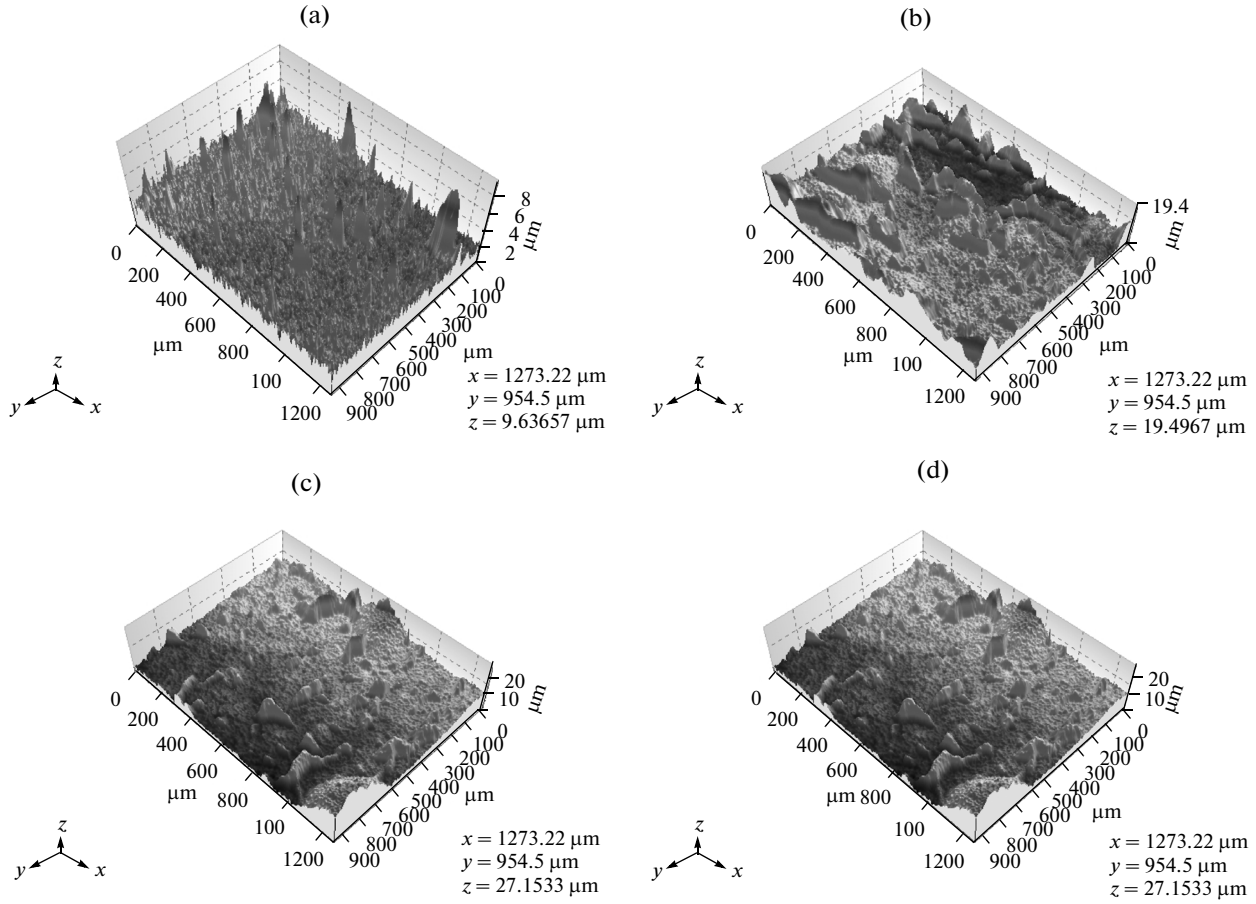

Fig. 5. 3D optical reconstructed surfaces by confocal microscopy of niobium oxide coating on steel alloy substrates: (a) pure substrate, (b) 230, (c) 280, and (d) 404 nm thin films.

tions were also calculated. The surface roughness increased with films up to 2 layers, and decreased in the 4-layered film as shown in Table 2, while the agglomerate diameter increased and then saturated. The maximum roughness behavior achieved in 2 layers deposition can be explained by the high viscosity of polymeric solution and also to difference on thermal behavior between film and substrate. While the increase in the roughness is expected as the films get thicker [32], its decrease of the 4-layered films can be assumed by the hypothesis that, at this point, due to the high viscosity, the Nb_2O_5 on the surface becomes a bulk material instead of remaining a film. Concerning the quality of the surface finish, the surface roughness/thickness ratio reached a maximum value for 2 layers deposition indicating very smooth film.

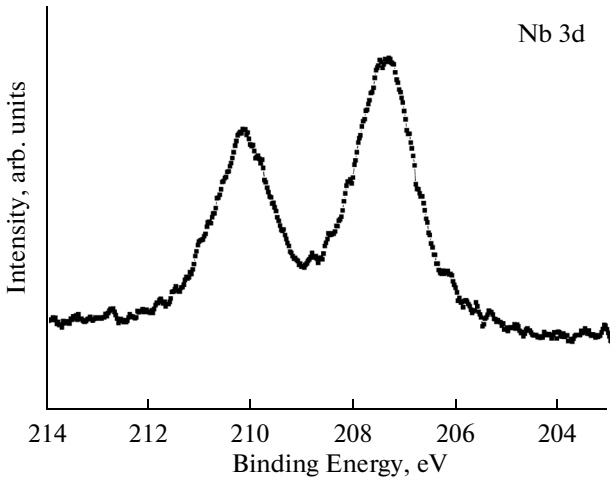

Fig. 6. XPS spectra of Nb $3d_{5/2}$ and Nb $3d_{3/2}$ orbitals for a niobium oxide coated on steel alloy substrates with 404 nm film thickn

The surface films were evaluated by XPS analyses in Fig. 6. The binding energy of Nb $3d_{5/2}$ and Nb $3d_{3/2}$ was approximately 203–205 and 207–208 eV, respectively. The presence of Nb oxides on the surface of the steels alloy caused a decrease in corrosion rate due to a decrease in the interfacial reaction kinetics. This suggests that the corrosion resistance was also improved as a result of film thickness.

Figure 7 presents the impedance spectra in the form of Nyquist plots obtained from the low alloy steel specimens with different film thickness, highlighting

Table 2. Values of average roughness, mean and standard deviation for each of the deposition conditions

Condition	Sample	Ra, μm	Mean value, μm	Standard deviation
No deposition	1	0.250	0.251	0.010
	2	0.262		
	3	0.242		
1 layer	1	0.413	0.367	0.040
	2	0.342		
	3	0.346		
2 layers	1	1.249	1.096	0.151
	2	0.947		
	3	1.092		
4 layers	1	0.808	0.709	0.085
	2	0.661		
	3	0.658		

the region of high frequencies. The increase in the diameter of the arc indicated an improvement in the film and charge transfer resistance. This suggests that higher film thickness promotes the formation of a passive film. This is important because it indicates good corrosion resistance. For thinner films, the progression of the corrosion rate of the steels is much higher. As the film thickness gowns, the corrosion rates decreased showing that the addition of Nb_2O_5 improves the corrosion behavior of low alloy steel and has better corrosion performance. This causes the film layer to become thicker and more compact. Therefore, the difference in corrosion rate is caused by the difference in composition and quantity of corrosion products formed on the steel surface. The rust formed is certainly dense enough to protect the steel during long exposure to the environment, which may suppress the anodic dissolution of steels. The corrosion resistance in the thicker film is due to the presence of niobium oxide, and to the enrichment of the steel surface with increasing of Nb concentration. Therefore, the corrosion rate in the case of Nb steels is strongly inhibited by the improvement of the film.

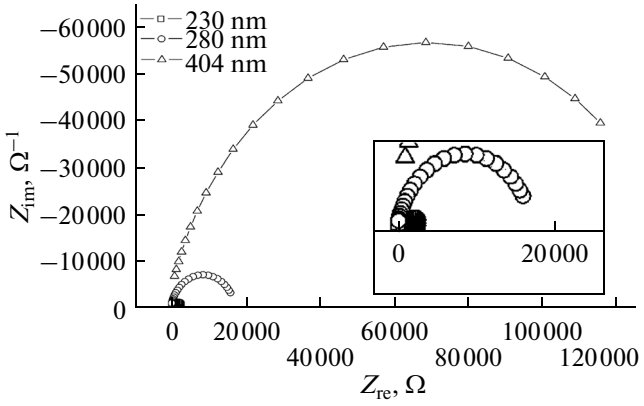

Fig. 7. EIS spectra of niobium oxide coated on steel alloy substrates with different thicknesses.

However, in a real situation, it is desired a material with good mechanical properties also. As discussed before, the results in Fig. 3 clearly show that the film with 2 layers exhibit a better mechanical behavior, in comparison with the other conditions. The less internal strain accounts for a more resistant, cohesive film. So, for the sake of analyzing a better condition for processing this thin film in industry, and by trading off those properties, it is logical to assume that, even if the electrochemical behavior of the film with 2 layers isn't the best, it is the optimal condition for an eventual production in oil and gas industry.

4. CONCLUSIONS

Crystalline niobium oxide films have been prepared by the polymeric precursor method on steel alloy substrates. The thickness effect on corrosion resistance properties of niobium oxide films fabricated by the polymeric precursor method was investigated. From the XRD measurements it was found that the films were crystalline with a composition very close to stoichiometric Nb_2O_5, suggesting deposition from a polymeric precursor solution. EIS showed that the charge transfer resistance increased with film thickness, indicating higher corrosion resistance. Moreover, from the point of view of corrosion resistance not all the deposition conditions were equivalent. For example the corrosion porosity factor changed by two orders of magnitude for specific deposition conditions, suggesting that some films had much fewer defects and thus provided better corrosion protection even though the physical-chemical properties were indistinguishable. The thinner film leads to a reduction of resistance corrosion as well as a decrease in grain size due to the internal strain resulting from the substrate/film interfacial layer. The optimal film thickness is close to 300 nm. The thicker film presents better resistance corrosion as a result of high internal strain, but the intermediate condition (2 layers) showed a better mechanical behavior. Therefore, for practical applications an optimal thickness value should be considered, taking into account these two properties.

ACKNOWLEDGMENTS

The authors gratefully acknowledge the financial support of the Brazilian financing agencies FAPESP, CNPq and CAPES.

REFERENCES

1. Guo, J., Yang, S., Shang, C., et al., *Corros. Sci.*, 2008, vol. 51, p. 242.
2. Melchers, R.E., *Corros. Sci.,* 2003, vol. 45, p. 2609.
3. Chen, X.J., Dong, E., and Han, W., *Mater. Lett.*, 2007, vol. 61, p. 4050.
4. Tahara, A. and Shinohara, T., *Corros. Sci.*, 2005, vol. 47, p. 2589.
5. Kamimura, T. and Stratmann, M., *Corros. Sci.,* 2001, vol. 43, p. 429.
6. Misawa, T., Asami, K., Hashimoto, K., and Shimodaira, S., *Corros. Sci.*, 1974, vol. 4, p. 279.
7. Nishimura, T., Katayama, H., Noda, K., and Kodama, T., *Corros. Sci.*, 2000, vol. 42, p. 1611.
8. Jang, Y.W., Hong, J.H., and Kim, J.G., *Met. Mater. Int.*, 2009, vol. 15, p. 623.
9. Murayama, M., Nishimura, T., and Tsuzaki, K., *Corros. Sci.*, 2008, vol. 50, p. 2159.
10. Chen, Y.Y., Tzeng, H.J., Wei, L.I., et al., *Corros. Sci.*, 2005, vol. 47, p. 1001.
11. Geneve, D., Rouxel, D., Pigeat, P., and Confente, M., *Corros. Sci.*, 2010, vol. 52, p. 1155.
12. Itagaki, M., Nozue, R., Watanabe, K., et al., *Corros. Sci.*, 2004, vol. 46, p. 1301.
13. Garet, M., Brass, A.M., Haut, C., and Solana, F.G., *Corros. Sci.*, 1998, vol. 39, p. 1073.
14. Nam, N.D., Kim, M.J., Yang, Y.W., and Kim, J.G., *Corros. Sci.*, 2010, vol. 52, p. 14.
15. Koch, G.H. and Rosenberg, H.S., in *Metals Handbook. Corrosion*, ASM Int., 1998, vol. 13, p. 1004, 9th ed.
16. Usami, A., Okushima, M., Sakamoto, S., et al., in *Nippon Steel Technical Report*, 2004, vol. 90, p. 25.
17. Meyer, L., Heisterkamp, F., and Mueschenborn, W., in *Proc. Conf. Microalloying'75*, New York, NY: Union Carbide, 1977, vol. 75, p. 153.
18. Hoogendoorn, T.M. and Spanraft, M.J., in *Proc. Conf. Microalloying'75*, New York, NY: Union Carbide, 1977, vol. 75, p. 75.
19. Gray, J.M., Levine, E., and Hill, D.C., *Weld. Res. Counc. Bull.*, 2005, vol. 213.
20. Yan, H., Bi, H., Li, X., and Xua, Z., *Mater. Charact.*, 2009, vol. 60, p. 204.
21. Fujita, N., Bhadeshia, H., and Kikuchi, M., *Mater. Sci. Eng.*, 2004, vol. 12, p. 273.
22. Fujita, N., Ohmura, K., and Yamamoto, A., *Mater. Sci. Eng., A*, 2003, vol. 351, p. 272.
23. Yazawa, Y. and Ozaki, Y., *JSAE Rev.*, 2003, vol. 24, p. 483.
24. Bard, A.J., Parsons, R., and Jordan, J., *Standard Potentials in Aqueous Solution*, New York: Marcel Dekker, 1985, p. 213.
25. Pourbaix, M., *Atlas of Electrochemical Equilibria in Aqueous Solutions*, New York: Pergamon, 1966.
26. Felton, E.J., *J. Less-Common Met.*, 1996, vol. 9, p. 206.
27. Velten, D., Eisenbarth, E., Schanne, N., and Breme, J., *J. Mater. Sci. Mater. Med.*, 2004, vol. 15, p. 457.
28. Foschini, C., Ramirez, M., Simões, S., et al., *Ceram. Int.*, 2013, vol. 39, p. 2185.
29. Hayashi, T., Oji, N., and Maiwa, H., *J. Appl. Phys.*, 1994, vol. 33, p. 5277.
30. Nagarajan, S., Raman, V., and Rajendran, N., *Mater. Chem. Phys.*, 2010, vol. 119, p. 363.
31. Joint Committee on Powder Diffraction Standards Database, International Centre for Diffraction Data.
32. Simões, A.Z., Zaghete, M.A., Cilense, M., et al., *J. Eur. Ceram. Soc.*, 2001, vol. 21, p. 1151.